

# Spatial Distribution of Electrokinetically Driven Flow Measured by Micro-PIV (An Evaluation of Electric Double Layer in Microchannel)

by

Mitsuhisa ICHIYANAGI <sup>(1)</sup>, Koichiro SAIKI, Yohei SATO, Koichi HISHIDA

Department of System Design Engineering  
Faculty of Science and Technology, Keio University  
Hiyoshi 3-14-1, Kohoku-ku, Yokohama, 224-8522, JAPAN

<sup>(1)</sup>E-Mail: [ichiyalagi@mh.sd.keio.ac.jp](mailto:ichiyalagi@mh.sd.keio.ac.jp)

## ABSTRACT

The effect of varying pH on electrokinetically driven flow has been investigated by an optical measurement system using fluorescent submicron particles. The objectives of the present study are to establish quantitative measurements of electroosmotic velocity and zeta-potential, and to apply a spatially averaged time-resolved particle tracking velocimetry (SAT-PTV) technique to particle stacking affected by pH gradient. SAT-PTV can detect an unsteady microchannel flow, eliminating the errors associated with Brownian motion without losing temporal resolution.

A flow is driven by the electric field in a T-shaped microchannel that is comprised of a poly(dimethylsiloxane) (PDMS) chip and a fused silica cover glass. 500 nm diameter particles were included in buffer solutions. Electroosmotic velocity was obtained by subtracting particle electrophoretic velocity from the observed particle velocity, and the zeta-potential of particles and each wall was calculated by using electrophoretic and electroosmotic velocities, respectively. With increasing pH, electroosmotic velocity and the zeta-potential of glass and PDMS surface was increased due to deprotonation at each surface.

Figure 1 depicts time evolution of an accumulation of submicron particles affected by pH gradient. The uniform concentration of submicron particles was observed at  $t = 0$ . On application of electric field, particles were moved toward the left hand side region, which is confirmed by velocity profiles of in the transverse direction detected by SAT-PTV, as shown in figure 2. At  $t = 7.8$  s particles were accumulated along the interface between different pH buffer solutions. It is pointed out from these results that the electric potential may influence depletion or accumulation of submicron particles.

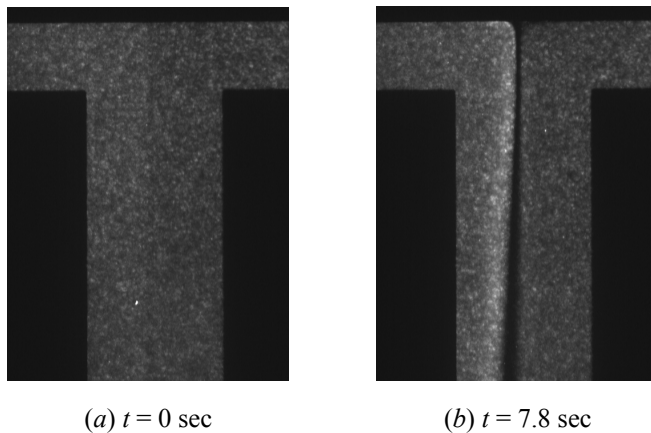


Figure 1. Instantaneous images of flow field in the junction area at (a)  $t = 0$  sec, (b)  $t = 7.8$  sec with the 600 V. HEPES buffer solution ( $pH = 7.2$ ) was injected into right hand side and Borate buffer solution ( $pH = 9.4$ ) was injected into left hand side.

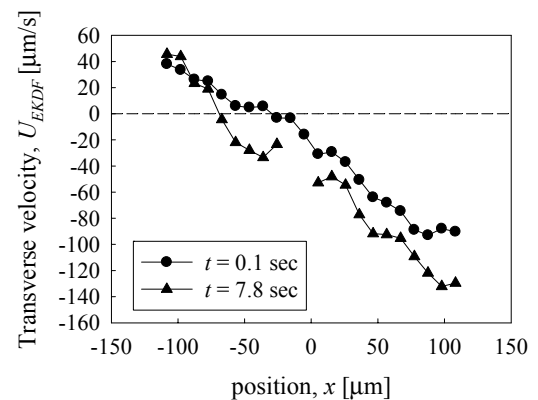


Figure 2. Transverse velocities versus transverse location ( $x$ ) at vertical location  $y = 150 \mu\text{m}$ .

## 1. INTRODUCTION

Rapid progress in micro- and nanotechnologies has contributed to develop a micro total analysis system (micro-TAS) that is realized on a-few-square-inches microfluidic devices. A number of complicated operations, which used to be carried out in a laboratory room using a-few-micro-liter reagent, are performed in a microchannel with a width of a few hundred  $\mu\text{m}$ . However, to date, the physics of transport process in microscale has not been precisely investigated, because of lack of quantitative measurement techniques with a high spatial resolution.

Electrokinetically driven flow is frequently observed in, for example, detection and separation operations, and has been qualitatively measured by fluorescence imaging. Experimental efforts using caged fluorescent dye (Paul *et al.* 1998, Ross *et al.* 2001) have shown the velocity distribution of electroosmotic flow in capillaries and microchannels, however, the influence of charged dye on velocity measurements has been vaguely discussed. Sato *et al.* (2002) investigated the three-dimensional structure of electroosmosis flow in an I-shaped microchannel by using micron-resolution particle image velocimetry (micro-PIV). Quantitative measurements of electrokinetically driven flow structure will advance our understanding, because the accurate control of electrokinetically driven flow is a key issue for the development of microminiaturized and integrated systems.

From a viewpoint of nanoscale, as a net charge close to the solid surface of a microchannel is created, an electric force can be used to drive a flow. In general, the positive ions are spontaneously attracted to the immobilized negative surface charges by electrostatic forces and stay in the vicinity of the surface, that is, the electric double layer is formed. The electroosmosis flow structure is governed by the formation of an electric double layer, because the electromigration of ions in the electric double layer induces the ion drag on the rest of liquid in a microchannel. The zeta-potential is equal to the potential drop in the electric double layer, so that measurements of the zeta-potential will extend our knowledge designing multifunctional microchannels and suppressing the loss in transport.

The objective of the present study is to investigate the effect of submicron particles and varying pH on the zeta-potential of the wall surface by using micro-PIV and spatially averaged time-resolved particle tracking velocimetry (SAT-PTV, Sato *et al.* 2003). Measurements are performed in a T-shaped microchannel, in which a flow is driven by an electric field.

## 2. VELOCITY MEASUREMENT TECHNIQUES

### 2.1 Measurement System

Figure 3 illustrates a schematic of the optical measurement system comprising an inverted microscope (Nikon Corp., TE300), a LD pumped solid-state CW laser ( $\lambda = 473 \text{ nm}$ ) and a 12-bit cooled CCD camera (Hamamatsu Photonics K. K., C4880-80) with a  $656 \times 494$  CCD array. The light source illuminates the microchannel by passing through a bandpass filter ( $\lambda = 450\text{--}490 \text{ nm}$ ) and a dichroic mirror reflecting wavelength below 505 nm. Fluorescence emitted from the submicron particles were collected on the CCD camera by passing through an oil immersion objective lens, a barrier filter transmitting wavelengths longer than 520 nm and a lens of a  $0.6 \times$  magnification. A  $10 \times$  magnification objective lens (Nikon Corp.) with numerical aperture of 0.5, a  $40 \times$  magnification objective lens (Nikon Corp.) with numerical aperture of 1.3, or a  $60 \times$  magnification objective lens (Nikon Corp.) with a numerical aperture of 1.4 were attached. The exposure time and frame interval of the CCD camera were 2 ms and 37 ms in the present study.

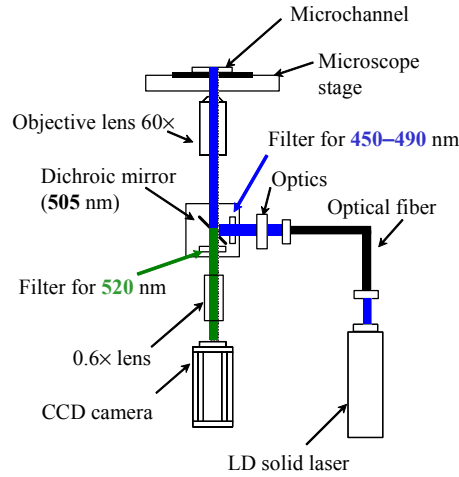


Figure 3. Schematic of the measurement system.

## 2.2 Submicron Particles and Buffer Solutions

Table 1 shows the properties of the fluorescent particles (Molecular Probes Inc.) used in the present study. Using fluorescent particles and the filter block (Figure 3) enables to eliminate scattered light generated by reflecting illumination at the microchannel surface. Diameter and density of fluorescent particles were selected to achieve high spatial resolution and not to bring about sedimentation in the buffer solutions. Since the carboxyl group ( $-\text{COOH}$ ) is added on the surface of the Submicron particles used in the present study, the surface is charged negatively in the buffer solutions. The measurement depth is calculated from the equation (1) [Meinhart *et al*, 2000].

$$\Delta z = \frac{3n\lambda_0}{NA^2} + \frac{2.16d_p}{\tan \theta} + d_p \quad (1)$$

where  $n$  is the refractive index of the fluid between the microchannel and the objective lens,  $\lambda_0$  is the wavelength of light,  $NA$  is the numerical aperture of the objective lens and  $d_p$  is the diameter of the particles. The Measurement depth for the 500 nm diameter particles is 8.6  $\mu\text{m}$  when using an objective of 10 $\times$  ( $NA=0.5$ ), 2.5  $\mu\text{m}$  when 40 $\times$  ( $NA=1.3$ ) and 2.2  $\mu\text{m}$  when 60 $\times$  ( $NA=1.4$ ).

Table 2 gives the fluid properties of buffer solutions used in the present study. Buffer solutions were used to allow adjustments to pH. Acetate buffer was used as acid buffer, HEPES buffer was used as neutral buffer, and Borate buffer was used as alkaline buffer. The molarity was coordinated to deflocculate submicron particles. The conductivity of each buffer solution is conformed by adding potassium chloride (KCl). Furthermore, submicron particles were added to each buffer solution with an amount of 0.2 % weight / volume.

Table 1 Properties of fluorescent particles

Material noun	polystyrene	
Diameter of particles	[nm]	500
Density	[g/cm <sup>3</sup> ]	1.055
Absorption wavelength	[nm]	505
Emission wavelength	[nm]	515

Table 2 Fluid properties

		Acetate	HEPES	Borate
Molarity	[mMol/l]	5	5	5
pH	[-]	4.7	7.1	9.4
Conductivity	[ $\mu\text{S/cm}$ ]	730	777	730

### 2.3 Micro-Resolution Particle Image Velocimetry (Micro-PIV)

The pioneering study of micro-PIV by Santiago *et al.* (1998) and Meinhart *et al.* (1999) conducted to obtain velocity vectors in microspace using fluorescent submicron particles with diameters of a few hundred nm as a flow tracer, which induces a measurement error associated with Brownian motion. Santiago *et al.* (1998) reduced the effect of Brownian motion on velocity detection by ensemble averaging and Meinhart *et al.* (1999) by ensemble-averaged correlation maps in time series.

### 2.4 Spatial Averaged Time-Resolved Particle Tracking Velocimetry (SAT-PTV)

A spatial averaged time-resolved particles tracking velocimetry (SAT-PTV, Inaba *et al.* 2001) method enables us to measure velocity variations in time series. The SAT-PTV method can eliminate the effect of Brownian motion by spatial averaging the velocities of each particle in a reference window of the PIV method.

Figure 4 exhibits schematics of the SAT-PTV method. The vector of the particle displacement between two successive images obtained by PTV,  $v_p$ , is comprised of a vector of the fluid flow,  $v_f$ , and a vector due to Brownian motion,  $v_B$ . When  $N$  particles are contained in an interrogation window where spatial averaging is performed, the SAT-PTV vector is expressed as follows:

$$\frac{1}{N} \sum_{\text{window}} v_p = \frac{1}{N} \sum_{\text{window}} v_f + \frac{1}{N} \sum_{\text{window}} v_B \quad (2)$$

As Brownian motion is statistically random and unbiased, an increase in the number of particles ( $N$ ) results in a zero value of the second term on the right hand side of equation (2). This means that the spatial-averaged vector of a particle displacement becomes equal to that of the fluid flow. Therefore it is possible to eliminate the effect of Brownian motion and obtain accurate vectors of the fluid flow in a time series. The time interval of the SAT-PTV system depends on the frame interval of the CCD camera (in this case 37 ms for a C4880-80).

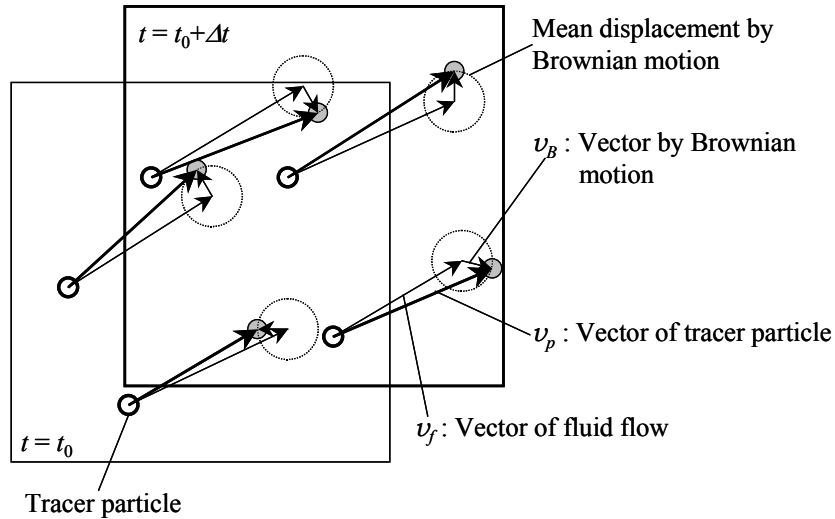


Figure 4. Schematics of the SAT-PTV method considering the effect of Brownian motion on velocity detection.

### 3. MEASUREMENTS OF ELECTROKINETICALLY DRIVEN FLOW

#### 3.1 Electrokinetically Driven Flow (EKDF)

Electrokinetically driven flow on a microscale includes electroosmotic flow (EOF) and electrophoresis (EP) as shown in Figure 5. Electroosmotic flow is the movement of liquid relative to a stationary charged surface (e.g., a capillary or a microchannel) resulting from an applied electric field (the movement to cathode as shown in Figure 5), while electrophoresis is the movement of a charged surface plus attached material (e.g., dissolved or suspended material) relative to the stationary liquid caused by the applied electric field (the movement to anode as shown in Figure 5). So the observed velocity of particles is summation of electroosmotic and electrophoretic velocity. These phenomena are caused by the electric double layer which consists of ions. The electric double layer is generated by charging at the liquid-solid interface positively or negatively and bringing about counter ions against the charged solid surface in the vicinity of the solid surface. Therefore, the electric potential of the solid surface governs electroosmotic and electrophoretic velocity, which is commonly called zeta-potential.

Figure 6 provides the flow chart for the calculation of the zeta-potential from the micro-PIV measurements. The observed velocities are summation of electroosmotic and electrophoretic velocities as given by equation (3) in Figure 6. Electroosmotic velocities are calculated by subtracting electrophoretic velocities from the observed velocities as given by equation (4) in Figure 6. Also, the theoretical electroosmotic velocity is calculated from the Navier-Stokes equation, the Boltzmann distribution, and the Poisson equation. The theoretical electroosmotic velocity is finally calculated from equation (5). Thus the zeta-potential on the surface is easily calculated from the experimental data by assigning permittivity and viscosity of the deionized water. This is justified since buffer solutions of low concentration were used.

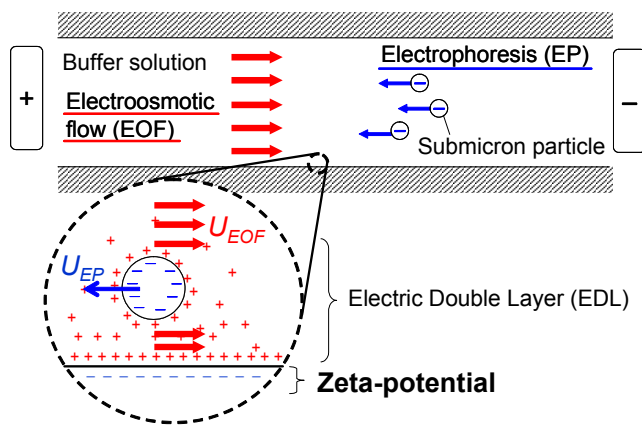


Figure 5. Schematic of electrokinetically driven flow.

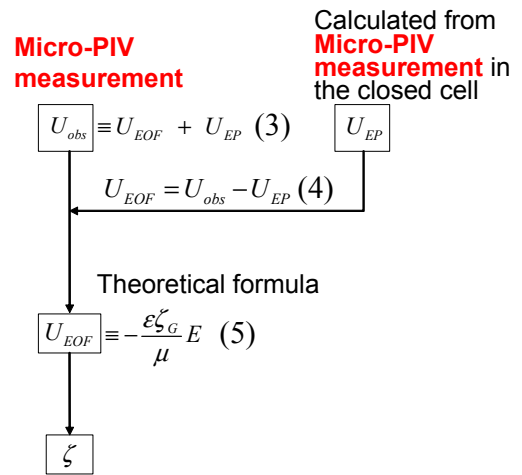


Figure 6. Calculation flow chart of zeta-potential. where  $\epsilon$  is permittivity,  $\zeta_G$  is zeta potential on the surface,  $E$  is electric field,  $\mu$  is viscosity.

#### 3.2 Electrophoretic Velocity of Particles

The electrophoretic velocities of 500 nm diameter particles in Acetate (pH = 4.7), HEPES (pH = 7.2) and Borate buffer solutions (pH = 9.4) were measured by using the closed cell shown in Figure 7 (Mori *et al*, 1980). The closed cell was comprised of a poly(dimethylsiloxane) (PDMS) chip and a cover glass. The PDMS chip was fabricated by using softlithography and the Pt thin film was applied on the cover glass by a sputtering machine (Plasma Sciences Inc., CrC-150). Applying an electric field in the closed cell results in a circulating flow in the depth-wise direction. This is caused by the motion of the buffer solution near the wall surface towards the cathode by electroosmotic flow and the motion of the buffer solution at the center of microchannel towards the anode.

Figure 8 shows the observed velocity profile of 500 nm diameter particles in Borate buffer solution measured by

micro-PIV. After the circulating flow induced by an electric field of 25 V/cm reaches a steady state, velocities at 14 measurement planes in the depth-wise direction were collected by using micro-PIV. This was achieved by shifting the measurement plane in the depth-wise direction in steps of 2  $\mu\text{m}$  which is equivalent to the measurement depth of 2.2  $\mu\text{m}$  for a 60  $\times$  magnification objective lens. The image size captured by the CCD camera is corresponding to a measurement area of 108  $\mu\text{m} \times 82 \mu\text{m}$ . Each velocity was calculated by averaging velocities of 100 subsequent images over a time period of 3.7 sec in addition to the spatial averaging performed for eliminating the effect of Brownian motion. Applying these results to the equations proposed by Mori and Okamoto (Mori *et al*, 1980) yields the electrophoretic velocities. Additionally, the theoretical electrophoretic velocity is calculated by the electrical force with the Stokes drag on the particle as given by equation (6).

$$U_{EP} = \frac{\epsilon \zeta_p}{\mu} E \quad (6)$$

where  $\zeta_p$  is zeta potential around submicron particles. Thus the zeta-potential around submicron particles is easily calculated from the experimental data by assigning permittivity and viscosity of deionized water.

Table 3 shows the zeta-potential around submicron particles and electrophoretic mobilities, which are obtained by dividing the electrophoretic velocities by the electric field strength. The surface of submicron particles is modified by the carboxyl group ( $-\text{COOH}$ ) which becomes ionized carboxyl group ( $-\text{COO}^-$ ) with an increase of pH, so that the number of hydrogen ions in the alkaline buffer solution becomes small and then the equilibrium of the carboxyl group ( $-\text{COOH} \rightleftharpoons -\text{COO}^- + \text{H}^+$ ) shifts to the right side. The ionized carboxyl group charges submicron particles negatively, and generates a zeta-potential around submicron particles. Therefore, these results imply that electrophoretic mobilities and zeta-potential increase with increasing pH.

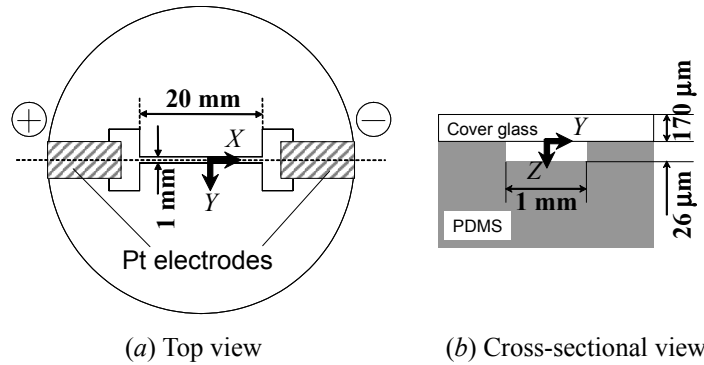


Figure 7. (a) Top view and (b) cross-sectional view of closed cell for measurements of electrophoretic velocity.

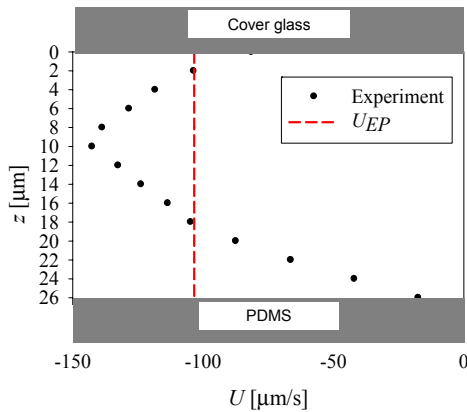


Figure 8. Electrophoretic velocity profile of 500 nm diameter particles in Borate buffer solution obtained for the closed cell with 25V/cm.

Table 3 Electrophoretic mobilities ( $u_{EP}$ ) and zeta-potential ( $\zeta_p$ ) of 500 nm diameter particles for varying pH

	Acetate	HEPES	Borate
$u_{EP}$ [ $\times 10^{-4}$ cm <sup>2</sup> /Vs]	-3.01	-3.82	-4.14
$\zeta_p$ [ $\times 10^{-3}$ V]	-38.6	-48.9	-53.0

### 3.3 An Evaluation of Electroosmotic Mobility and Zeta-potential

Electroosmotic velocities and zeta-potential of fused silica cover glass and PDMS surfaces in Acetate (pH = 4.7), HEPES (pH = 7.2) and Borate buffer solutions (pH = 9.4) were measured by using an I-shaped microchannel shown in Figure 9. The microchannel was comprised of a PDMS chip and fused silica cover glass. This experiment was performed by injecting each buffer solution including submicron particles into the microchannel. Adjusting to the heads between the inlet and outlet eliminates pressure driven flow. Pt electrodes were set to the inlet and outlet and an electric field of 55 V/cm. Observed velocities for both surfaces were obtained by averaging 300 images corresponding to an averaging time of 11.1 sec. Observed velocities of the PDMS surface were measured by shifting the measurement planes in the depth-wise direction to 80  $\mu\text{m}$  from the fused silica cover glass surface. The image size captured by the CCD camera is corresponding to a measurement area of 180  $\mu\text{m}$   $\times$  136  $\mu\text{m}$  by using a 60  $\times$  magnification objective lens ( $NA = 1.4$ ).

Table 4 shows the electroosmotic mobility and the zeta-potential of fused silica cover glass and PDMS surfaces in steady state, which were obtained from instantaneous velocities detected by SAT-PTV method. The spatial resolution is 13.8  $\mu\text{m}$   $\times$  13.8  $\mu\text{m}$   $\times$  2.2  $\mu\text{m}$  based on the size of the interrogation window and the measurement depth of the oil immersion objective lens ( $NA = 1.4$ ). The number of velocity vectors calculated in one instantaneous image is 20  $\times$  14. Electroosmotic mobilities and zeta-potential of both surfaces are calculated by averaging temporal and spatial velocities, respectively. The number of averaged velocity vectors is about 80000. Fused silica cover glass and PDMS surface is comprised of a chain of silanol group (SiOH). It means that the equilibrium of deprotonation ( $\text{SiOH} \rightleftharpoons \text{SiO}^- + \text{H}^+$ ) shifts to the right side in alkaline buffer solution. This implies that the silanol group on both surfaces is dissociated with an increase pH. The dissociated silanol group ( $\text{SiO}^-$ ) charges fused silica cover glass and PDMS surfaces negative, and generates zeta-potential on both surfaces. Therefore, table 4 shows that the electroosmotic mobility and the zeta-potential of both surfaces increase with increasing pH. Furthermore, RMS values of electroosmotic mobility and zeta-potential of both surfaces are obtained from about 80000 velocities. The RMS values of the electroosmotic mobility and the zeta-potential for the PDMS surface are larger than that for the fused silica cover glass. The surface roughness of the PDMS chip is larger than that of fused silica cover glass. Due to the disturbance of the particle motion by roughness, it is more difficult for the PDMS surface to correct for Brownian motion.

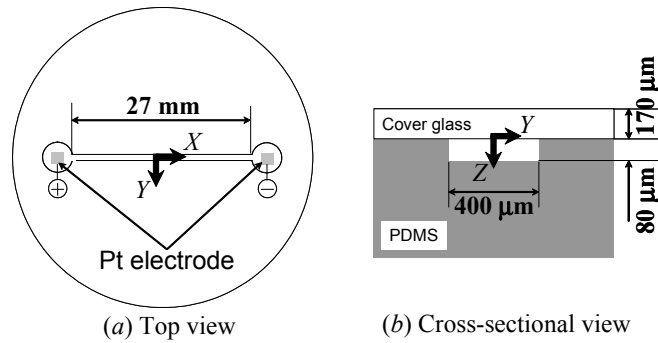


Figure 9. (a) Top view and (b) cross-sectional view of I-shaped microchannel.

Table 4 Electroosmotic mobilities ( $u_{EOF}$ ) and zeta-potential ( $\zeta_G$ ) on (a) fused silica cover glass and (b) PDMS surface detected by SAT-PTV.

	(a) Fused silica cover glass			(b) PDMS		
	Acetate	HEPES	Borate	Acetate	HEPES	Borate
$u_{EOF}$ [ $\times 10^{-4}$ cm <sup>2</sup> /Vs]	2.71 $\pm$ 0.06	4.69 $\pm$ 0.05	5.74 $\pm$ 0.09	1.34 $\pm$ 0.28	4.61 $\pm$ 0.11	5.81 $\pm$ 0.09
$\zeta_G$ [ $\times 10^{-3}$ V]	-35.5 $\pm$ 0.7	-57.9 $\pm$ 0.6	-69.5 $\pm$ 1.2	-17.2 $\pm$ 3.6	-59.0 $\pm$ 1.4	-74.4 $\pm$ 1.2

### 3.4 Effect of pH Gradient

Electrokinetically driven flow affected by a pH gradient was analyzed by using the T-shaped microchannel shown in Figure 10. A pH gradient was formed by injecting two buffer solutions with different pH-value simultaneously. The microchannel was comprised of a PDMS chip and fused silica cover glass. This experiment was performed by injecting HEPES buffer solution (pH = 7.2) including submicron particles into inlet A and Borate buffer solution (pH = 9.4) including submicron particles into inlet B. A pressure driven flow was generated by the heads between the inlet and outlet. Pt electrodes were set to the inlet and outlet and a voltage of 600 V was applied. Observed velocities were obtained by averaging 500 images corresponding to an averaging time of 18.5 sec. The image size captured by the CCD camera is corresponding to a measurement area of  $649 \mu\text{m} \times 489 \mu\text{m}$  by using a  $10 \times$  magnification objective lens ( $NA = 0.5$ ) and  $270 \mu\text{m} \times 204 \mu\text{m}$  by using a  $40 \times$  magnification objective lens ( $NA = 1.3$ ).

The uniform concentration of submicron particles at the T-junction prior to the application of an electric field is seen in Figure 11 (a), where the flow is pressure driven. With the application of 600 V between the horizontal inlets and the vertical outlet of the T-shaped microchannel, it is observed that an interface between HEPES buffer solution and Borate buffer solution is formed. The submicron particles concentrate at the left side of the interface in HEPES buffer solution as shown in Figure 11 (b) and (c). This accumulation is accompanied by a depletion of submicron particles in a region to the left side of the interface. A steady non-uniform submicron particles density field was formed after about 7 seconds from the application of the electric field.

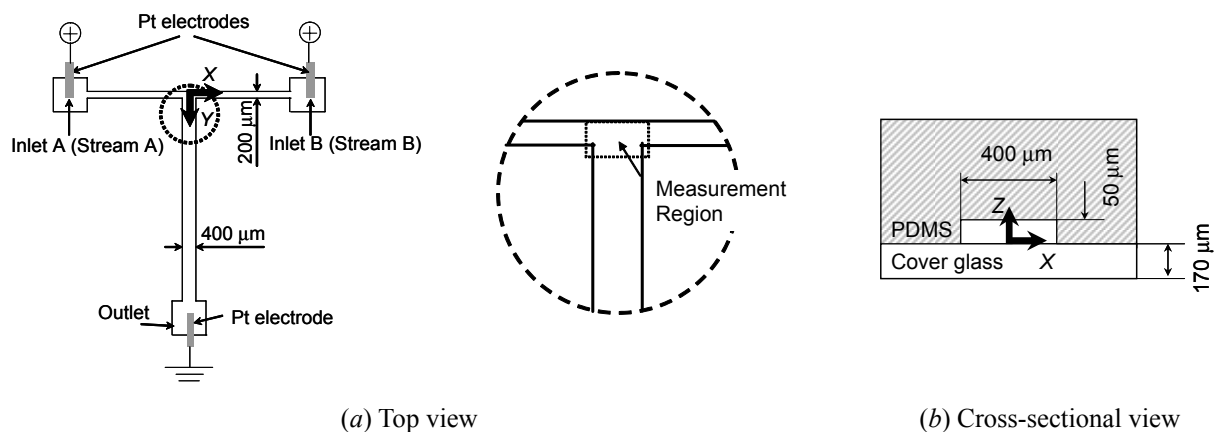


Figure 10. (a) Top view and (b) cross-sectional view of T-shaped microchannel.

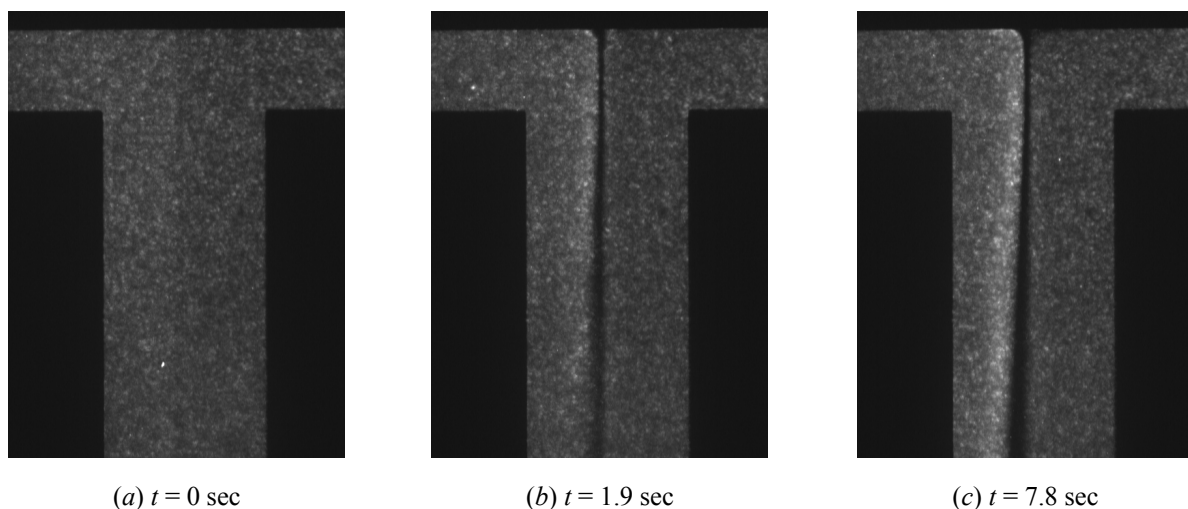


Figure 11. Instantaneous images of flow field in the junction area at (a)  $t = 0$  sec, (b)  $t = 1.9$  sec and (c)  $t = 7.8$  sec with the 600 V. HEPES buffer solution (pH = 7.2) including fluorescent submicron particles was injected into right hand side (inlet A) and Borate buffer solution (pH = 9.4) including fluorescent submicron particles was injected into left hand side (inlet B).

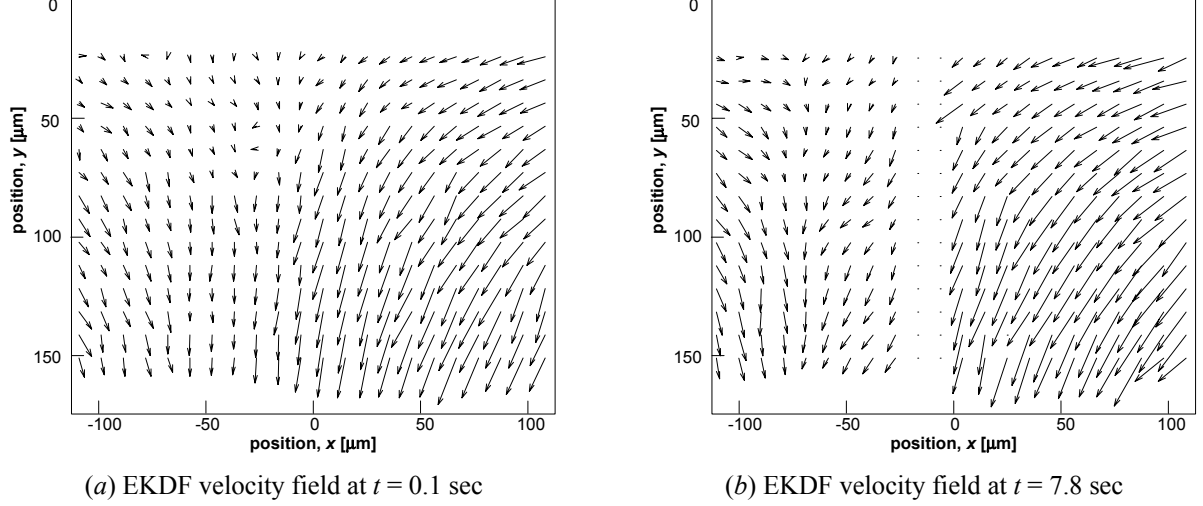


Figure 12. EKDF velocity vector field measured by using SAT-PTV (a) 0.1 sec and (b) 7.8 sec after applying a voltage of 600 V.

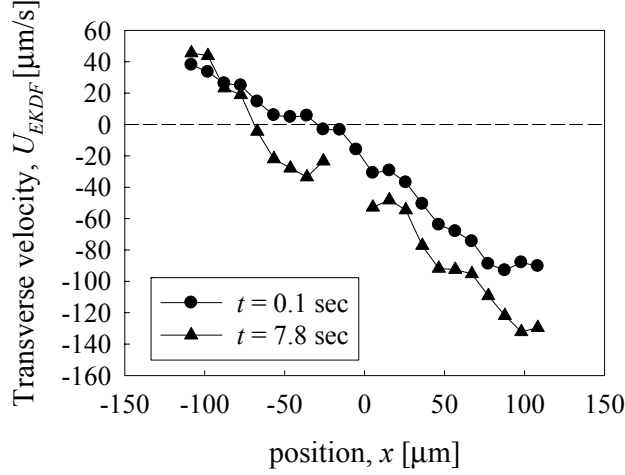


Figure 13. Transverse velocity versus transverse location ( $x$ ) at vertical location  $y = 150 \mu m$ .

Time-dependant two-dimensional measurements were conducted at one location along the streamwise direction which is the measurement region as shown in Figure 10(a) and at one depth which is the mid-plane of the microchannel ( $z = 25 \mu m$ ). The spatial resolution is  $13.8 \mu m \times 13.8 \mu m \times 2.5 \mu m$  based on the size of the interrogation window and the measurement depth of the oil immersion objective lens ( $NA = 1.3$ ). The number of velocity vectors calculated in one instantaneous image is  $22 \times 14$ . The observed velocity of the submicron particles  $U_{obs}$  consists of the components given in equation (7).

$$U_{obs} = U_{Pr} + U_{EOF} + U_{EP} \quad (7)$$

where  $U_{Pr}$  is the velocity of pressure driven flow,  $U_{EOF}$  is electroosmotic velocity, and  $U_{EP}$  is electrophoretic velocity. Therefore, electrokinetically driven flow (EKDF) velocity  $U_{EKDF}$  is calculated as given by equation (8), which is summation of electroosmotic and electrophoretic velocity.

$$U_{EKDF} = U_{obs} - U_{Pr} = U_{EOF} + U_{EP} \quad (8)$$

Figure 12 illustrate the EKDF velocity vector field measured by SAT-PTV at  $t = 0.1$  sec and  $t = 7.8$  sec after applying a voltage of 600 V. It is observed that there are no velocity vectors in transverse gap ranging from approximately  $x = -20 \mu m$  to  $0 \mu m$  (Figure 12 (a)). This region is corresponding to a region that there is few submicron particles by a depletion of submicron particles. Figure 13 gives transverse velocity of the EKDF velocities versus transverse location ( $x$ ) at vertical location  $y = 150 \mu m$ . The transverse velocities at  $t = 7.8$  sec shift to the down side than those at

$t = 0.1$  sec, where transverse velocity toward the right is defined as positive. Therefore, transverse velocities toward the left direction at  $t = 7.8$  sec are increased as compared with those at  $t = 0.1$  sec, especially at transverse location from  $x = -70 \mu\text{m}$  to  $-25 \mu\text{m}$ , the direction of the transverse velocities change from right to left. These locations are corresponding to a region of the accumulation of submicron particles. It can be seen that it is affected by electric potential that transverse velocities toward the left direction are increased.

#### 4. Conclusions

An experimental study to investigate the effect of submicron particles and varying pH on zeta-potential of the wall surface was performed. Zeta-potential of the wall surface and around submicron particles is significantly affected by varying pH of buffer solutions, inducing an increase in electroosmotic and electrophoretic velocities increase with an increasing pH. Particle stacking affected by pH gradient in the T-shaped microchannel was investigated by SAT-PTV. On application of electric field particles were moved toward the left hand side region and finally particles were accumulated along the interface between different pH buffer solutions. It can be concluded from these results that the electric potential may influence depletion or accumulation of submicron particles.

#### ACKNOWLEDGEMENTS

This work was subsidized by the Grant-in-Aid for Scientific Research of Ministry of Education, Culture, Sports, Science and Technology (No. 14702030 and 15206024).

#### REFERENCES

- Abe, M., Yoshida, N., Hishida, K. and Maeda, M. (1998). "Multilayer PIV technique with high power pulse laser diodes", Proc. 9th Int. Symp. Appl. Laser Tech. Fluid Mech., CD-ROM
- Badal, M.Y., Wong, M., Chiem, N., Salimi-Moosavi, H. and Herrison, D.J. (2002). "Protein separation and surfactant control of electroosmotic flow in poly(dimethylsiloxane)-coated capillaries and microchips", J. Chromatography A, 947, pp. 277-286.
- Beyon, R.J. and Easterby, J.S. (1996). Buffer Solutions, The Basics, IRL Press.
- Buch, J.S., Wang, P.C., Devoe, D.L. and Lee, C.S. (2001). "Field-effect flow control in a polydimethylsiloxane- based microfluidic system", Electrophoresis, 22, pp. 3902-3907.
- Devasenathipathy, S., Santiago, J.G., Yamamoto, T., Sato, Y. and Hishida, K. (2003). "Electrokinetic Particle Separation", Micro Total Analysis Systems 2003, 1, pp. 845-848.
- Inaba, S., Sato, Y., Hishida, K. and Maeda, M. (2001). "Flow Measurements in Microspace Using Sub-Micron Fluorescent Particles—An Effect of Brownian Motion on Velocity Detection—", Proc. Fourth Int. Symp. *Particle Image Velocimetry*, 1141.
- Meinhart, C.D., Wereley, S.T., Santiago, J.G. (1999). "PIV measurements of a micro channel flow", Exp. Fluids, Vol. 27, pp. 414-419.
- Meinhart, C.D., Wereley, S.T. and Gray, H.B. (2000). "Volume illumination for two-dimensional particle image velocimetry", Meas. Sci. Technol., 11, pp. 809-814.
- Mori, S. and Okamoto, H. (1980). "A Unified Theory of Determining the Electrophoretic Velocity of Mineral Particles in the Rectangular Micro-Electrophoresis Cell", Fusen, Vol. 27, pp. 117-126.

- Ocvirk, G., Munroe, M., Tang, T., Oleschuk, R., Westra, K. and Harrison, D.J. (2001). "Electrokinetic control of fluid in native poly(dimethylsiloxane) capillary electrophoresis devices", *Electrophoresis*, 21, pp. 107-115.
- Oddy, M.H. and Santiago, J.G. (2004). "A method for determining electrophoretic and electroosmotic mobilities using AC and DC electric field particle displacements", *J. Colloid and Interface Science*, 269, pp. 192-204
- Paul, P.H., Garguilo, M.G. and Rakestraw, D.J. (1998). "Imaging of Pressure- and Electrokinetically Driven Flows through Open Capillaries", *Anal. Chem.*, Vol. 70, pp. 2459-2467.
- Probstein, R.F. (1994). *Physicochemical Hydrodynamics, An Introduction* second edition, John Wiley & Sons.
- Ross, D., Johnson, T.J. and Locascio, L.E. (2001). "Imaging of Electroosmotic Flow in Plastic Microchannels", *Anal. Chem.*, Vol. 73, pp. 2509-2515.
- Santiago, J.G. (2002). *Fluid Flow in Micro Devices*, Stanford Univ.
- Santiago, J.G., Werely, S.T., Meinhart, C.D., Beebe, D.J. and Adrian, R.J. (1989). "A Particle Image Velocimetry System for Microfluidics", *Exp. Fluids*, Vol. 25, pp. 316-319.
- Sato, Y., Hishida, K. and Maeda, M. (2002). "Quantitative Measurement and Control of Electrokinetically Driven Flow in Microspace", *Micro Total Analysis Systems 2002*, 1, pp. 512-514.
- Sato, Y., Inaba, S., Hishida, K. and Maeda, M. (2003). "Spatially averaged time-resolved particle-tracking velocimetry in microspace considering Brownian motion of submicron fluorescent particles", *Exp. Fluids*, Vol. 35, pp. 167-177.
- Scales, P.J., Grieser, F. and Healy, W. (1992). "Electrokinetics of the Silica-Solution Interface: A Flat Plate Streaming Potential Study", *Langmuir*, 8, pp. 965-974.
- Spehar, A.M., Koster, S., Linder, V., Kulmala, S., Rooij, N.F., Sigrist, H. and Thormann, W. (2003). "Electrokinetic characterization of poly(dimethylsiloxane) microchannels", *Electrophoresis*, 24, pp. 3674-3678.
- Sze, A., Erickson, D., Ren, L. and Li, D. (2003). "Zeta-potential measurement using the Smoluchowski equation and the slope of the current-time relationship in electroosmotic flow", *J. Colloid and Interface Science*, 261, pp. 402-410.
- Tsuda, T., Ikedo, M., Jones, G., Daddo, R. and Zare, R.N. (1993). "Observation of flow profiles in electroosmosis in a rectangular capillary", *J. Chromatography*, Vol. 632, pp. 201-207.
- Yamamoto, T., Inaba, S., Sato, Y., Hishida, K. and Maeda, M. (2002). "Measurements in microchannel by laser induced molecular tagging and micro-PIV", *Proc. 11th Int. Symp. Appl. Laser Tech. Fluid Mech.*, CD-ROM